



**CHALMERS**  
UNIVERSITY OF TECHNOLOGY

## **Fast Charging Control of Lithium-Ion Batteries: Effects of Input, Model, and Parameter Uncertainties**

Downloaded from: <https://research.chalmers.se>, 2025-07-03 06:11 UTC

Citation for the original published paper (version of record):

Cai, Y., Zou, C., Li, Y. et al (2022). Fast Charging Control of Lithium-Ion Batteries: Effects of Input, Model, and Parameter Uncertainties. 2022 European Control Conference, ECC 2022: 1647-1653.  
<http://dx.doi.org/10.23919/ECC55457.2022.9838024>

N.B. When citing this work, cite the original published paper.

# Fast Charging Control of Lithium-Ion Batteries: Effects of Input, Model, and Parameter Uncertainties

Yao Cai, Changfu Zou, Yang Li, and Torsten Wik

**Abstract**—The foundation of advanced battery management is computationally efficient control-oriented models that can capture the key battery characteristics. The selection of an appropriate battery model is usually focused on model order, whereas the effects of input and parameter uncertainties are often overlooked. This work aims to pinpoint the minimum model complexity for health-conscious fast charging control of lithium-ion batteries in relation to sensor biases and parameter errors. Starting from a high-fidelity physics-based model that describes both the normal intercalation reaction and the dominant side reactions, Padé approximation and the finite volume method are employed for model simplification, with the number of control volumes as a tuning parameter. For given requirements on modeling accuracy, extensive model-based simulations are conducted to find the simplest models, based on which the effects of current sensor biases and parameter errors are systematically studied. The results show that relatively low-order models can be well qualified for the control of voltage, state of charge, and temperature. On the other hand, high-order models are necessary for health management, particularly during fast charging, and the choice of the safety margin should also take the current sensor biases into consideration. Furthermore, when the parameters have a certain extent of uncertainties, increasing the model order will not provide improvement in model accuracy.

## I. INTRODUCTION

Lithium-ion (Li-ion) batteries are one of the most commonly used energy storage devices thanks to their high energy density, low self-discharge rate, and ever-declining costs [1], [2]. In order to ensure safe use and prolong the lifetime of Li-ion batteries, proper models are vital for various battery management functionalities. The most investigated battery models are the equivalent circuit models, which use circuit elements to mimic the voltage-current characteristics of the battery cells. These models have relatively simple mathematical structures and low computation requirements [3]. However, such a model is empirical and lacks the capability to simulate or predict the battery's internal behaviors, albeit the information is critical for healthy and safe battery management [4].

In contrast, in an electrochemical model, a set of partial differential equations are used to describe the charging and discharging processes inside the cells. One of the most popular electrochemical models of Li-ion batteries is the pseudo-two-dimensional (P2D) model [5]. One dimension is along the particle radius as the porous electrodes are assumed

to be composed of many spherical particles. The other dimension is along the cell thickness. Since the width and the length of a cell are much larger than its thickness, this model describes the dynamic behavior only along the thickness [6]. To solve the P2D model for the purposes of real-time control and management, discretization can be used, both in the time and space domains. In general, increasing the spatial discretization volumes can increase the accuracy of the model, but it also leads to increased computational burden. In this work, we consider fixed numbers of discretized volumes in the radial direction, as well as in the separator domain, while the numbers of the positive and negative electrode domains are varied, depending on the use.

Since the full-order P2D model is too computationally demanding for online use in a battery management system (BMS), many attempts to model simplification have been made. Some research focuses on reducing the number of particles. By assuming that each entire electrode depth can be represented by one particle, and the governing equations can be significantly simplified, leading to the single particle model (SPM) with the least computational requirement. However, the SPM has many preconditions. Most notably, it leads to large errors at high current rates and/or with thick electrodes [6] [7].

When increasing the particle number from one in the SPM to only two or three, the output errors can be greatly reduced while the increased computational demand is still fairly modest. External constraints on current and terminal voltages are widely used for designing charging strategies today. There are a number of studies exhibiting the potential benefits of using additional cell internal constraints for healthier and faster charging [8]–[10]. For example, the charging could be significantly accelerated with reduced the risk of lithium plating by keeping the overpotential above a safety threshold. The reason for the threshold is to have a safety margin to cope with model prediction errors. To maximize the benefits, the errors should therefore be as small as possible. However, there is no point to further reduce the discretization errors if the effects from other sources, such as measurement errors and parameter uncertainties, are significant.

This study aims to find the effects of different model configurations on the performance of the P2D model under different battery operating conditions. In addition to the discretization errors, two external factors that can cause model inaccuracy are also taken into consideration, including the current sensor and the parameter uncertainties. The cells are cycled with the hybrid pulse power characterization (HPPC) test [11] or constant charging test. Aiming at es-

This work was supported by the Swedish Energy Agency (Grant No. P42787-1).

All the authors are with the Department of Electrical Engineering, Chalmers University of Technology, Gothenburg, 41296, Sweden (E-mail: yao.cai@chalmers.se; changfu.zou@chalmers.se; yangli@ieee.org; tw@chalmers.se).

establishing low order models, first, we investigate output errors when the number of particles varies from 1 to 10, and the maximum difference (with signs) during the whole time/period is calculated, to compare with the 1% error requirement for the offline model. When it comes to the inputs, the analysis focuses on their effects on the major causes of battery degradation: Lithium plating and growth of the solid-electrolyte interphase (SEI) layer. To study how the parameter uncertainties affects the system, a parameter analysis is done with respect to all six outputs, including measured target variables and control target ones. With all these results, the effects of inputs, model and parameter uncertainties on fast charging control of Li-ion batteries are jointly evaluated.

## II. EXTERNAL EFFECTS ON DIFFERENT PARTICLES MODEL

### A. Battery Model

A schematic of a typical Li-ion battery cell is shown in Fig. 1. In the P2D model, there are three domains, including the cathode, separator, and anode, denoted by the symbol +, sep, and -, respectively. During the charging and discharging process of the battery, lithium ions travel through the separator between the cathode and the anode back and forth, causing the concentration ( $c$ ) of lithium ions, the current density ( $i$ ), the potential ( $\Phi$ ) and other physical quantities to change. The corresponding dynamic behaviors can be described by a series of partial differential-algebraic equations (PDAEs) [5], where the superscript  $j \in \{+, sep, -\}$ ,  $\pm \in \{+, -\}$ .

In electrolyte of the two electrodes and the separator:

$$\frac{\partial c_e^j(x, t)}{\partial t} = \frac{1}{\varepsilon_e^j} \frac{\partial}{\partial x} \left( D_{e, \text{eff}}^j \frac{\partial c_e^j(x, t)}{\partial x} \right) + \frac{t_a^0}{F \varepsilon_e^j} \frac{\partial i_e^j(x, t)}{\partial x} \quad (1)$$

$$\frac{\partial \Phi_e^j(x, t)}{\partial x} = -\frac{i_e^j(x, t)}{\kappa_{\text{eff}}^j} + \frac{2R_g T(t) t_a^0}{F} \left( 1 + \frac{d \ln f_c/a}{d \ln c_e} \right) \times \frac{\partial \ln c_e^j(x, t)}{\partial x} \quad (2)$$

$$\frac{\partial i_e^\pm(x, t)}{\partial x} = F a_s^\pm j_{\text{tot}}^\pm(x, t) \quad (3)$$

$$\frac{\partial i_e^{\text{sep}}(x, t)}{\partial x} = 0 \quad (4)$$

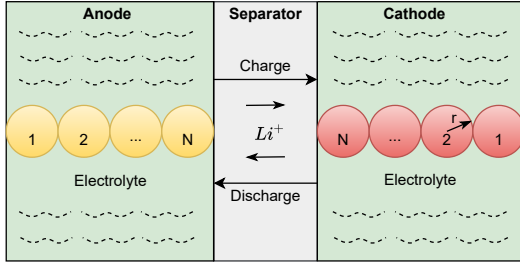


Fig. 1. 1D schematic of a Li-ion battery cell with  $N$  particles in each electrode. From left to right, the three compartments represent the anode, separator, and cathode, respectively.

In the two electrodes:

$$\frac{\partial c_s^\pm(x, r, t)}{\partial t} = \frac{1}{r^2} \frac{\partial}{\partial r} \left( D_{s, \text{eff}}^\pm r^2 \frac{\partial c_s^\pm(x, r, t)}{\partial r} \right) \quad (5)$$

$$\frac{\partial \Phi_s^\pm(x, t)}{\partial x} = -\frac{i_s^\pm(x, t)}{\sigma_{\text{eff}}^\pm} \quad (6)$$

$$\frac{\partial i_s^\pm(x, t)}{\partial x} = -F a_s^\pm j_{\text{tot}}^\pm(x, t) \quad (7)$$

$$j_{\text{int}}^\pm(x, t) = \frac{i_0^\pm(x, t)}{F} \left[ \exp \left( \frac{\alpha F \eta_{\text{int}}^\pm(x, t)}{R_g T(t)} \right) - \exp \left( -\frac{(1-\alpha) F \eta_{\text{int}}^\pm(x, t)}{R_g T(t)} \right) \right] \quad (8)$$

$$= \frac{2i_0^\pm(x, t)}{F} \sinh \left( \frac{F \eta_{\text{int}}^\pm(x, t)}{2R_g T(t)} \right)$$

$$i_0^\pm(x, t) = F k_{\text{eff}}^\pm \sqrt{c_e^\pm(x, t) (c_{s, \text{max}}^\pm - c_{\text{ss}}^\pm(x, t)) c_{\text{ss}}^\pm(x, t)} \quad (9)$$

$$\eta_{\text{int}}^\pm(x, t) = \Phi_s^\pm(x, t) - \Phi_e^\pm(x, t) - U_{\text{ss}}^\pm(x, t) - F r_f^\pm j_{\text{tot}}^\pm(x, t) \quad (10)$$

$$U_{\text{ss}}^\pm(x, t) = U^\pm(c_{\text{ss}}^\pm) + \frac{\partial U^\pm}{\partial T} (T(t) - T_{\text{ref}}) \quad (11)$$

where the physical meanings of the symbols are given at the end of this work, and the boundary and initial conditions are omitted here for the sake of brevity. A standard way of simulating the P2D model is to use the finite volume method. In the P2D model, either along the thickness direction or the radial direction, for each discretized volume, the gradients of the variables at both the center point and at the edges are needed, so the method of lines can be applied [12]. Here, we consider the number of discretized volumes in the positive and the negative electrode are the same and denoted by  $N$ , and the corresponding model is denoted as an  $N$ -particle model.

### B. Current Sensor Bias

Note that in the P2D model, the applied current density is the model input, specified in the boundary conditions. Measurement errors are inevitable in current sensors, not the least in vehicle applications where costs are kept at a minimum. Nowadays, the measurement errors after calibration are 2% and 0.5% for the shunt-based and Hall-based current sensors used in electric vehicles, respectively [13]. Here, we compare the errors caused by the sensor bias with the output errors caused by the reduction of the particle numbers. To comply with these error specifications, we investigate four levels of bias, i.e., -2%, -0.5%, 0.5%, and 2%.

### C. Parameter Uncertainties

Since the electrochemical model of the Li-ion battery is derived from the chemical phenomena inside the cell during the charging and discharging processes, it has a large set of parameters that describe the characteristics of a cell. Some of the parameters can be accurately measured and considered to have no error, such as the current collector parameters. The parameters related to the battery degradation and some thermal behaviors will not be discussed in this work. To study how the uncertainties in the remaining, unmeasured

parameters can affect the model outputs, the sensitivity matrix will first be calculated and the parameters will be next ranked according to how sensitive the selected outputs are to each of the parameters [14]. Consider a general nonlinear relationship between the input and the output,

$$y = f_{\theta}(u), \quad (12)$$

where  $y \in \mathbb{R}^{n_y}$  is the vector consisting of selected outputs, normalized with corresponding maximum values under no parameter perturbations.  $u \in \mathbb{R}$  is the input to the model and  $\theta \in \mathbb{R}^{n_{\theta}}$  represents the vector of parameters. The sensitivity derivative matrix  $S \in \mathbb{R}^{n_y \times n_{\theta}}$  of the model outputs to the parameter vector is defined as

$$\begin{aligned} S &\equiv \frac{\partial f_{\theta}}{\partial \theta}(u) = [S_1, S_2, \dots, S_{n_{\theta}}] \\ &= \left[ \frac{\partial f_{\theta}}{\partial \theta_1}(u), \frac{\partial f_{\theta}}{\partial \theta_2}(u), \dots, \frac{\partial f_{\theta}}{\partial \theta_{n_{\theta}}}(u) \right] \\ &\cong \left[ \frac{f_{\theta_1} - f_{\theta}}{\Delta \theta_1}(u), \frac{f_{\theta_2} - f_{\theta}}{\Delta \theta_2}(u), \dots, \frac{f_{\theta_{n_{\theta}}} - f_{\theta}}{\Delta \theta_{n_{\theta}}}(u) \right]. \end{aligned} \quad (13)$$

If the level of parameter uncertainty is unknown, we may assume an equal bias to all the parameters, which means that all the elements in  $S$  share the same denominator. In (13),  $S_i$  represents the sensitivity of all the outputs to the  $i$ th parameter. One can obtain a measure of the total effect of the different parameters by using the Euclidean norm. First, we calculate the values of  $\|S_i\|$ ,  $\forall i$ , rank the results in descending order, and then form a diagonal matrix  $D$  using the ranked sequence, i.e.,

$$D = \begin{bmatrix} \|S_1\| & 0 & \dots & 0 \\ 0 & \|S_2\| & \dots & 0 \\ \vdots & \vdots & \ddots & \vdots \\ 0 & 0 & \dots & \|S_{n_{\theta}}\| \end{bmatrix}. \quad (14)$$

Having the ranking matrix  $D$ , a linear dependence matrix  $C$  can be calculated by solving the decomposition equation  $S^T S = D^T C D$  [15], expressed by

$$C = \begin{bmatrix} 1 & \frac{\langle S_1, S_2 \rangle}{\|S_1\| \|S_2\|} & \dots & \frac{\langle S_1, S_{n_{\theta}} \rangle}{\|S_1\| \|S_{n_{\theta}}\|} \\ \frac{\langle S_2, S_1 \rangle}{\|S_2\| \|S_1\|} & 1 & \dots & \frac{\langle S_2, S_{n_{\theta}} \rangle}{\|S_2\| \|S_{n_{\theta}}\|} \\ \vdots & \vdots & \ddots & \vdots \\ \frac{\langle S_{n_{\theta}}, S_1 \rangle}{\|S_{n_{\theta}}\| \|S_1\|} & \frac{\langle S_{n_{\theta}}, S_2 \rangle}{\|S_{n_{\theta}}\| \|S_2\|} & \dots & 1 \end{bmatrix}. \quad (15)$$

Each element  $\frac{\langle S_i, S_j \rangle}{\|S_i\| \|S_j\|}$  of  $C$  is by definition between  $-1$  and  $1$  according to the Cauchy-Schwartz inequality, and it is a measure of linear dependence between the two parameters  $\theta_i$  and  $\theta_j$ . The larger the absolute value of  $\frac{\langle S_i, S_j \rangle}{\|S_i\| \|S_j\|}$  is, the stronger the linear dependence the two parameters have. With the matrices  $D$  and  $C$ , we have measures of both the parameter sensitivity and the linear dependence between any two parameters. If the uncertainties can be acquired from the

manufacturer or the experience, a new sensitivity deviation matrix can be calculated by scaling the constant parameter bias  $S$  matrix, i.e.,

$$S_u = S U, \quad (16)$$

where

$$U = \begin{bmatrix} \theta_{1u} & 0 & \dots & 0 \\ 0 & \theta_{2u} & \dots & 0 \\ \vdots & \vdots & \ddots & \vdots \\ 0 & 0 & \dots & \theta_{\theta_{n_u}} \end{bmatrix},$$

and  $\theta_{iu}$  is the specified uncertainty of the  $i$ th parameter. Replacing  $S$  by  $S_u$  in (14) and (15), the corresponding updated matrices  $D_u$  and  $C_u$  can be derived. By multiplying with the uncertainty matrix,  $\|S_i\|$  is exactly the norm of the changes of the  $i$ th output because of the uncertainties of the parameters. The norm of the output changes caused by the current sensor bias or the reduced number of particles can also be calculated in a similar way.

#### D. Output Errors

In this work, with a given input sequence, the accuracy of  $N$ -particle model is evaluated by the normalized maximum error  $\delta$  compared to the benchmark, defined by

$$\delta[\%] = \text{sign}(y_N - y_{\text{benchmark}}) \left| \max \left( \frac{y_N - y_{\text{benchmark}}}{y_{\text{benchmark}}} \right) \right| * 100\%$$

### III. RESULTS AND DISCUSSION

In this section, the method described above is applied under the input current profile of HPPC test and constant charging. The particle number  $N$  under investigation changes from 1 to 10. The results from a 100-particle model are used as the benchmark.

#### A. HPPC

First, the HPPC test is conducted. The results for the 6 chosen outputs are shown in Table I. When the number of particles of each electrode is three, the maximum deviations in voltage, temperature, SOH, and SOC are all within 1%, which satisfies the requirements of the offline model. Since the SEI layer growth and the lithium plating can harm the cell's health, they need particular focus. It can be seen that, for  $N = 3$ , the maximum lithium plating deviation is as high as  $-5.4186\%$  and in order to achieve the target of 1% error, nine particles are needed for each electrode. Furthermore, the maximum SEI layer thickness deviation decreases to below 1% only when the number of particles increases to seven.

1) *Current sensor noise*: Since the lithium plating only occurs when the lithium plating overpotential is negative, it is dangerous to overestimate the overpotential. So instead of analyzing the unsigned maximum deviation, as (II-D), the maximum positive errors are studied.

Fig. 2a shows the lithium plating errors under different scenarios compared with the benchmark. The blue, red, and yellow bars represent the output errors of the SPM to the 10-particle model with  $-2\%$ ,  $2\%$ , and zero input current biases, respectively. It can be seen that When the number of particles increases, the yellow and the blue bars have a

TABLE I

MODEL ERRORS WITH DIFFERENT PARTICLE NUMBERS UNDER HPPC PROFILE

Particle No.	V[%]	T[%]	Lip[%]	SEI[%]	SOH[%]	SOC[%]
1	-2.5382	-1.7102	-15.1908	3.8708	-1.3927	0.0346
2	-1.6459	0.7997	-9.1381	2.9998	-0.6916	0.0089
3	-0.9502	0.3472	-5.4186	2.1473	-0.4561	0.0089
4	-0.7143	0.1900	-3.3982	1.6558	-0.3385	0.0134
5	-0.5733	0.1208	-2.2745	1.3405	-0.2679	0.0140
6	-0.4779	0.0825	-1.7463	1.1205	-0.2209	0.0112
7	-0.4083	0.0597	-1.4141	0.9601	-0.1873	0.0210
8	-0.3556	0.0454	-1.1627	0.8381	-0.1621	0.0119
9	-0.3140	0.0357	-0.9731	0.7404	-0.1426	0.0136
10	-0.2801	0.0288	-0.8248	0.6629	-0.1269	0.0198

decreasing trend. However, The results cannot be used as the reference to select a safe margin because they do not represent the worst case.

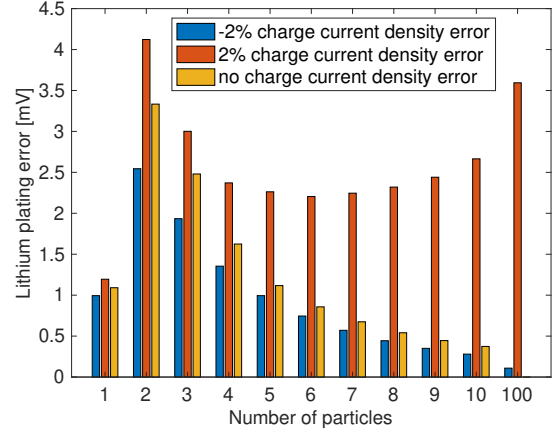
After studying the impacts of the 2% current bias, the same process is applied to the model with the more accurate current sensor, which can reach 0.5% accuracy after calibration. The results of lithium plating errors are presented in Fig. 2b. In this case, all the three bars' heights decrease monotonically as the number of particles increases from 1 to 10. Similarly to Fig. 2a, we see that when the number of particles is larger than one the red bars are always higher than the others. Hence, when selecting the safety margin, one should always use the red bars as the reference.

When it comes to the SEI layer growth, it is of interest to study the SEI layer thickness increment in the long term. Fig. 3a shows the SEI layer thickness increment after 10 HPPC charging-discharging test in the current sensor without bias, or with bias of  $-2\%$ ,  $-0.5\%$ ,  $0.5\%$  and  $2\%$ . Included are also simulations for the number of particles ranging from 1 to 10 together with the benchmark. That is, there are  $5 \times 11 = 55$  curves in the figure. However, as can be seen in the zoom, all the lines are very close to each other. The 55 lines have only a range of around  $5 \times 10^{-10}$  m, which is less than 1% of the total SEI layer thickness increment. This may seem contradictory to the large percentage listed in Table I, where we can see large errors at the very beginning of the cycle while the SEI layer increment is close to zero. This means that the denominator used in the calculation is very small. Fig. 3b shows all the 55 scenarios' errors in percentage and, clearly, that all the lines go below 1% after a few hours. For SEI layer prediction, the impacts of the model order and the current sensor bias are not significant after the very first beginning.

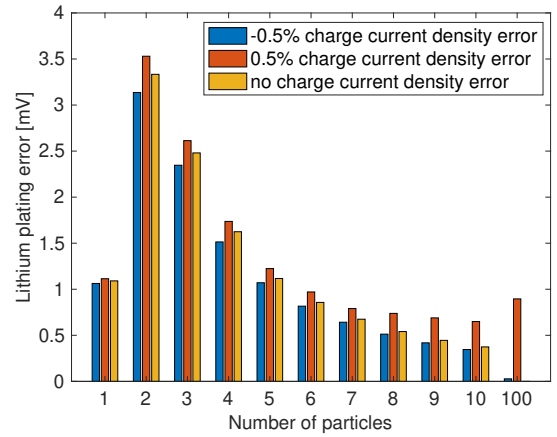
2) *Parameter sensitivity analysis*: There are around one hundred predefined parameters in the P2D model. Four groups of parameters were selected for the parameter sensitivity analysis, i.e.,

- 1) Geometric parameters:  $R_p^+$ ,  $L^+$ ,  $\varepsilon_e^+$ ,  $\varepsilon_s^+$ ,  $R_p^-$ ,  $L^-$ ,  $\varepsilon_e^-$ ,  $\varepsilon_s^-$ ,  $L^{sep}$ ,  $\varepsilon_e^{sep}$ ,  $A$
- 2) Transport parameters:  $D_s^+$ ,  $\sigma^+$ ,  $D_s^-$ ,  $\sigma^-$ ,  $D_e$ ,  $t^+$
- 3) Kinetic parameters:  $k_{eff}^+$ ,  $k_{eff}^-$ ,  $Brugg$
- 4) Concentration parameters:  $c_{s,max}^+$ ,  $c_{s,max}^-$ ,  $c_e^0$

First, we assume all parameters have  $\pm 1\%$  error and calculate the corresponding norms in the ranking matrix. The



(a)



(b)

Fig. 2. (a) Absolute errors of lithium plating potential under (a) constant current charging and (b) HPPC profile.

12 highest ranked parameters are listed in Table II. All the remaining parameters have  $\|S_i\|$  less than 0.01.

The results in Table II show that the parameter that has the most significant effects on the outputs is electrode surface area  $A$ , followed by solid maximum ionic concentration  $c_{s,max}^-$  in the negative electrode, active material volume fraction  $\varepsilon_s^-$  of the negative electrode, the thickness of the negative electrode  $L^-$ , and the electrolyte volume fraction  $\varepsilon_e^-$  of the negative electrode, and the active material volume fraction  $\varepsilon_s^+$  of the positive electrode. The corresponding  $C$  matrix for the six most influential parameters is:

$$C = \begin{matrix} & A & c_{s,max}^- & \varepsilon_s^- & L^- & \varepsilon_e^- & \varepsilon_s^+ \\ \begin{matrix} A \\ c_{s,max}^- \\ \varepsilon_s^- \\ L^- \\ \varepsilon_e^- \\ \varepsilon_s^+ \end{matrix} & \begin{pmatrix} 1.00 & 0.96 & 0.96 & 0.95 & 0.80 & 0.25 \\ 0.96 & 1.00 & 1.00 & 1.00 & 0.80 & -0.03 \\ 0.96 & 1.00 & 1.00 & 1.00 & 0.80 & -0.03 \\ 0.95 & 1.00 & 1.00 & 1.00 & 0.77 & -0.04 \\ 0.80 & 0.80 & 0.80 & 0.77 & 1.00 & -0.05 \\ 0.25 & -0.03 & -0.03 & -0.04 & -0.05 & 1.00 \end{pmatrix} \end{matrix} \quad (17)$$

Furthermore, it can be noticed that  $A$ ,  $c_{s,max}^-$ ,  $\varepsilon_s^-$ , and  $\varepsilon_e^-$  are highly correlated to each other.

TABLE II  
12 PARAMETERS WITH THE HIGHEST SENSITIVITY WHEN UNCERTAINTY IS AND IS NOT CONSIDERED

Symbol	Physical Meaning	Unit	Without Uncertainty			With Uncertainty	
			HPPC $\ S_i\ $	Constant Charg- ing $\ S_i\ $	Approx. Uncertain- ties[%]	HPPC $\ S_i\ $	Constant Charg- ing $\ S_i\ $
$A$	Electrode plate area	$\text{m}^2$	2.6899	3.1315	$\pm 1.5$	0.0403	0.0470
$c_{s,\max}^-$	Negative electrode solid maximum concentration	$\text{mol}/\text{m}^3$	2.4266	2.9088	$\pm 5$	0.1213	0.1454
$\varepsilon_s^-$	Negative electrode active material volume fraction	m	2.3830	2.8920	$\pm 5$	0.1191	0.1446
$L^-$	Negative electrode thickness	m	2.2032	2.7172	$\pm 1.5$	0.0330	0.0408
$\varepsilon_e^-$	Electrolyte volume fraction in the negative electrode	-	0.9723	1.1396	$\pm 5$	0.0486	0.0570
$\varepsilon_s^+$	Positive active material volume fraction	-	0.7103	0.7631	$\pm 5$	0.0355	0.0382
$c_{s,\max}^+$	Positive electrode solid maximum concentration	$\text{m}^3$	0.7102	0.7631	$\pm 4$	0.0284	0.0305
$L^+$	Positive electrode thickness	m	0.7047	0.7664	$\pm 1.5$	0.0106	0.0115
$Brugg$	Bruggman coefficient	-	0.6957	0.9880	$\pm 20$	0.1391	0.1976
$\varepsilon_e^+$	Electrolyte volume fraction in the positive electrode	-	0.1787	0.5325	$\pm 5$	0.0089	0.0266
$R_p^-$	Negative particle radius	m	0.1388	0.0977	$\pm 20$	0.0278	0.0195
$t_a^0$	Transference number of lithium cation	-	0.1074	0.1571	$\pm 10$	0.0107	0.0157

In Table II, the expected parameter uncertainties for different parameters are presented. Taking the parameter uncertainty into consideration and using (17), the ranking changes significantly, see Table II. The corresponding  $C$  matrix for the six most influential parameters is:

$$C_u = \begin{pmatrix} Brugg & c_{s,\max}^- & \varepsilon_s^- & \varepsilon_e^- & A & \varepsilon_s^+ \\ Brugg & \begin{pmatrix} 1.00 & -0.78 & -0.78 & -0.98 & -0.75 & 0.11 \\ -0.78 & 1.00 & 1.00 & 0.80 & 0.96 & -0.03 \\ -0.78 & 1.00 & 1.00 & 0.80 & 0.96 & -0.03 \\ -0.98 & 0.80 & 0.80 & 1.00 & 0.80 & -0.05 \\ -0.75 & 0.96 & 0.96 & 0.80 & 1.00 & 0.25 \\ 0.11 & -0.03 & -0.03 & -0.05 & 0.25 & 1.00 \end{pmatrix} \end{pmatrix} \quad (18)$$

Next, we calculate the norm of maximum output changes due to the current sensor bias. From the previous result, we select the worst case with 2% bias and select the three-particle model, i.e., the same as the model used for the sensitivity analysis. The result is 0.0258, which ranks 10 among all parameters tested. Then we calculate the norm of the maximum output changes when the number of particles decreases from 10 to 3. The result 0.0183, which is also ranked 10 among all parameters. This means that the uncertainties of the parameters are worth more attention.

### B. Constant Charging

Repeating all the steps as described above under the constant charging at 1C, the output errors between models with different particle numbers and the benchmark are listed in Table III. A similar analysis can be applied here.

For the lithium plating overpotential, it can be seen in Fig. 4a and Fig. 4b that the currents with -2% and -0.5% bias cause the largest errors under this constant charging. When it comes to the SEI layer thickness, Fig. 5a shows that the difference caused by the current sensor bias is much smaller than the SEI layer thickness increment. Though the error in percentage is large, there is a trend of decreasing error percentages with time (see Fig. 5b).

As for the sensitivity analysis, the results are listed in Table II and the linear dependence matrices are:

TABLE III  
MODEL ERRORS WITH DIFFERENT PARTICLE NUMBERS UNDER 1C  
CONSTANT CHARGING

Particle No.	V[%]	T[%]	Lip[%]	SEI[%]	SOH[%]	SOC[%]
1	1.9943	-1.2238	79.4588	-35.1103	-0.4435	0.0148
2	0.9870	0.4241	11.2455	-20.2329	-0.2283	-0.0060
3	0.6513	0.1479	6.4393	-14.9988	-0.1496	-0.0024
4	0.4834	0.0785	4.1803	-11.8069	-0.1108	-0.0013
5	0.3827	0.0496	2.9290	-9.6855	-0.0877	-0.0008
6	0.3156	0.0341	2.1626	-8.1791	-0.0723	-0.0006
7	0.2676	0.0248	1.6595	-7.0558	-0.0613	-0.0004
8	0.2316	0.0187	1.3120	-6.1867	-0.0530	-0.0003
9	0.2037	0.0146	1.0621	-5.4945	-0.0466	-0.0003
10	0.1813	0.0119	0.8766	-4.9303	-0.0415	-0.0002

$$C = \begin{pmatrix} A & c_{s,\max}^- & \varepsilon_s^- & L^- & \varepsilon_e^- & Brugg \\ A & \begin{pmatrix} 1.00 & 0.99 & 0.99 & 0.98 & 0.74 & -0.70 \\ 0.99 & 1.00 & 1.00 & 1.00 & 0.70 & -0.63 \\ 0.99 & 1.00 & 1.00 & 1.00 & 0.70 & -0.63 \\ 0.98 & 1.00 & 1.00 & 1.00 & 0.64 & -0.58 \\ 0.74 & 0.70 & 0.70 & 0.64 & 1.00 & -0.86 \\ -0.70 & -0.63 & -0.63 & -0.58 & -0.86 & 1.00 \end{pmatrix} \end{pmatrix} \quad (19)$$

$$C_u = \begin{pmatrix} Brugg & c_{s,\max}^- & \varepsilon_s^- & \varepsilon_e^- & A & L^- \\ Brugg & \begin{pmatrix} 1.00 & -0.63 & -0.63 & -0.86 & -0.70 & -0.58 \\ -0.63 & 1.00 & 1.00 & 0.70 & 0.99 & 1.00 \\ -0.63 & 1.00 & 1.00 & 0.70 & 0.99 & 1.00 \\ -0.86 & 0.70 & 0.70 & 1.00 & 0.74 & 0.64 \\ -0.70 & 0.99 & 0.99 & 0.74 & 1.00 & 0.98 \\ -0.58 & 1.00 & 1.00 & 0.64 & 0.98 & 1.00. \end{pmatrix} \end{pmatrix} \quad (20)$$

From this, we calculate that the rankings are the same as for the HPPC cycles. From matrix  $C$ , it can also be seen that the correlation relationship between different parameters is very similar as well. Similar to the HPPC test but with a current bias of -2%, which is the worst case in the constant charging test, the norm of maximum output changes due to the current sensor bias is 0.0258, which ranks 10 among all parameters tested. The norm of maximum output changes when the number of particles decreases from 10 to

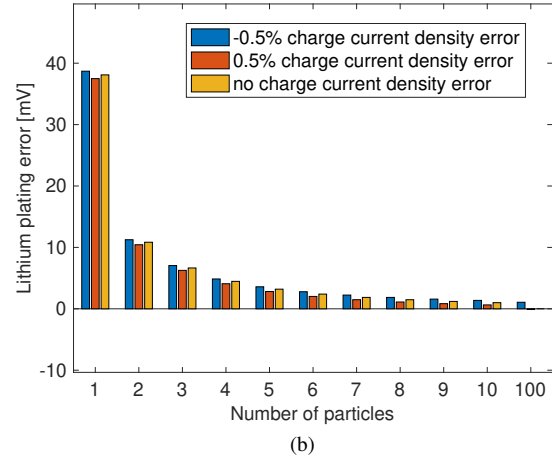
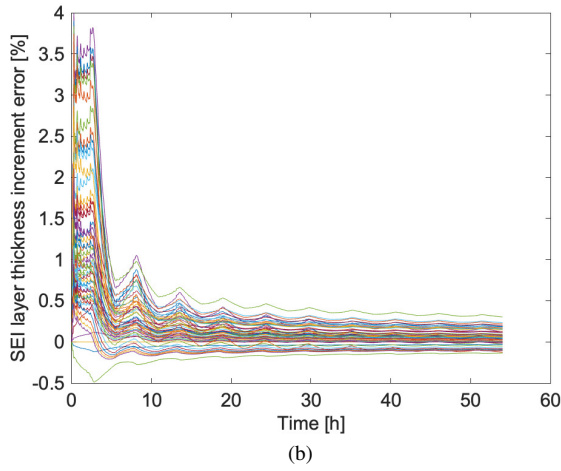
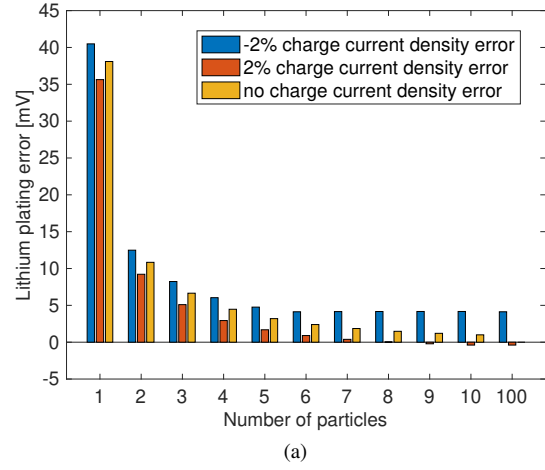
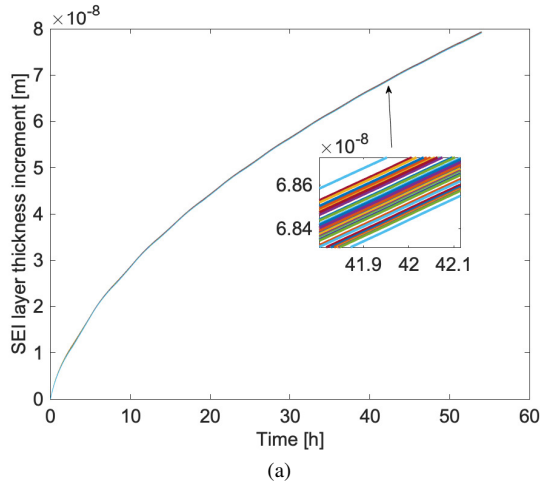


Fig. 3. Increment error of SEI layer thickness (a) SEI layer thickness increment error in meter. (b) SEI layer thickness increment error in percentage.

Fig. 4. Lithium plating error under constant charging considering the current sensor bias of (a)  $\pm 2\%$  and (b)  $\pm 0.5\%$ .

3 is 0.0106, which is ranked 11 among all parameters. This also means the uncertainties of the parameters need more attention.

#### IV. CONCLUSION

The concluding remarks of this work are summarized as follows. Generally, the more particles the model uses, the more accurate results can be achieved. Though, for the terminal voltage, temperature, SOH, and SOC, already two- or three-particle model can satisfy the offline model's requirement to limit the error to be less than 1%. From this perspective, a large number of particles is not necessary. However, for the control target variables we selected, the lithium plating overpotential and the SEI layer thickness, a low number of particles is not accurate enough. When it comes to the input biases, for the lithium plating overpotential it makes sense to compare the maximum error to the benchmark. Adding the biases from the current sensor, it can be concluded that the current sensor biases can influence the choice of the safety margin a lot. That is, to be able to use different size model, a proper safety margin is needed, which

takes not only the number of particles but also the current sensor bias into consideration. For the SEI layer thickness, model size and current sensor bias can be ignored because their error range is too small compared with the growth of the SEI layer. With the results of the parameter analysis, the most sensitive parameters can be found with or without knowing the parameter uncertainties, and so can the correlation between them as well. After comparing the sensitivity norm of the output changes caused by the reduction of the number of particles, as well as the current sensor bias, it can be found the reduction of particles number does not affect the output as much as the parameter uncertainties. This also holds for the current sensor bias, though it is larger than that of the reduction of number of particles. This means if considering some of the measure target variables and some important control target variables together, the parameter uncertainties affect the outputs much more than a reduction of the number of particles. If the parameter uncertainties of one battery cannot be reduced to a lower standard compared with that in the paper, then increasing the model order is not helpful to reduce the output error. Knowing this information, further

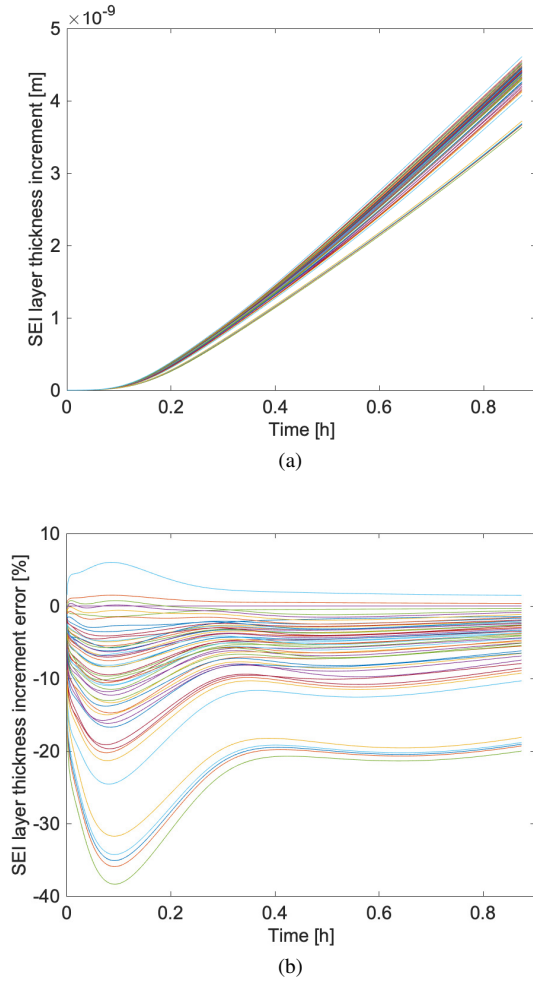


Fig. 5. SEI layer thickness increment error in (a) SI unit and (b) percentage.

parameter identification work emphasized particularly on the sensitive parameters is needed.

## REFERENCES

- [1] B. Dunn, H. Kamath, and J.-M. Tarascon, "Electrical energy storage for the grid: A battery of choices," *Sci.*, vol. 334, no. 6058, pp. 928–935, 2011.
- [2] B. A. Johnson and R. E. White, "Characterization of commercially available lithium-ion batteries," *J. Power Sources*, vol. 70, no. 1, pp. 48–54, 1998.
- [3] C. Zou, C. Manzie, D. Nešić, and A. G. Kallapur, "Multi-time-scale observer design for state-of-charge and state-of-health of a lithium-ion battery," *J. Power Sources*, vol. 335, pp. 121–130, 2016.
- [4] G. L. Plett, *Battery Management Systems, Volume I: Battery Modeling*. Artech House, 2015.
- [5] Y. Li, D. Karunathilake, D. M. Vilathgamuwa, Y. Mishra, T. W. Farrell, S. S. Choi, and C. Zou, "Model order reduction techniques for physics-based lithium-ion battery management: A survey," *IEEE Ind. Electron. Mag.*, 2021.
- [6] N. A. Chaturvedi, R. Klein, J. Christensen, J. Ahmed, and A. Kojic, "Algorithms for advanced battery-management systems," *IEEE Control Syst. Mag.*, vol. 30, no. 3, pp. 49–68, 2010.
- [7] N. T. Tran, M. Vilathgamuwa, Y. Li, T. Farrell, S. S. Choi, and J. Teague, "State of charge estimation of lithium ion batteries using an extended single particle model and sigma-point Kalman filter," in *2017 IEEE Southern Power Electron. Conf.*, 2017, pp. 1–6.
- [8] C. Zou, X. Hu, Z. Wei, T. Wik, and B. Egardt, "Electrochemical estimation and control for lithium-ion battery health-aware fast charging," *IEEE Trans. Ind. Electron.*, vol. 65, no. 8, pp. 6635–6645, 2018.

- [9] Y. Li, M. Vilathgamuwa, E. Wikner, Z. Wei, X. Zhang, T. Thiringer, T. Wik, and C. Zou, "Electrochemical model-based fast charging: Physical constraint-triggered PI control," *IEEE Trans. on Energy Convers.*, vol. 36, no. 4, pp. 3208–3220, Dec. 2021.
- [10] L. Wikander, B. Fridholm, S. Gros, and T. Wik, "Ideal benefits of exceeding fixed voltage limits on lithium-ion batteries with increasing cycle age," *J. Power Sources*, vol. 441, p. 227179, 2019.
- [11] C. Zou, X. Hu, S. Dey, L. Zhang, and X. Tang, "Nonlinear fractional-order estimator with guaranteed robustness and stability for lithium-ion batteries," *IEEE Trans. Ind. Electron.*, vol. 65, no. 7, pp. 5951–5961, 2017.
- [12] M. Torchio, L. Magni, R. B. Gopaluni, R. D. Braatz, and D. M. Raimondo, "LIONSIMBA: A Matlab framework based on a finite volume model suitable for Li-ion battery design, simulation, and control," *J. Electrochem. Soc.*, vol. 163, 2016.
- [13] K. Maniar, *Comparing shunt- and hall-based isolated current-sensing solutions in HEV/EV*, SBAA293B–June 2018–Revised January 2019 ed., Texas Instruments Incorporated, 2019.
- [14] H. Christopher Frey and S. R. Patil, "Identification and review of sensitivity analysis methods," *Risk analysis*, vol. 22, no. 3, pp. 553–578, 2002.
- [15] B. F. Lund and B. A. Foss, "Technical communique: Parameter ranking by orthogonalization-applied to nonlinear mechanistic models," *Automatica*, vol. 44, no. 1, p. 278–281, jan 2008. [Online]. Available: <https://doi.org/10.1016/j.automatica.2007.04.006>

## LIST OF SYMBOLS

- $\Phi_s$ : solid-phase potential [V]  
 $\Phi_e$ : electrolyte potential [V]  
 $i_s$ : solid-phase current density [ $A \cdot m^{-2}$ ]  
 $i_e$ : electrolyte current density [ $A \cdot m^{-2}$ ]  
 $i_0$ : exchange current density [ $A \cdot m^{-2}$ ]  
 $c_s$ : solid-phase concentration [ $mol \cdot m^{-3}$ ]  
 $c_{s,max}$ : theoretical maximum solid-phase concentration [ $mol \cdot m^{-3}$ ]  
 $c_{ss}$ : surface concentration of solid-particle [ $mol \cdot m^{-3}$ ]  
 $c_e$ : electrolyte concentration [ $mol \cdot m^{-3}$ ]  
 $c_e^0$ : average electrolyte concentration [ $mol \cdot m^{-3}$ ]  
 $j_{tot}$ : total molar flux [ $mol \cdot m^{-2} \cdot s^{-1}$ ]  
 $j_{int}$ : intercalation molar flux [ $mol \cdot m^{-2} \cdot s^{-1}$ ]  
 $\eta_{int}$ : activation overpotential for intercalation [V]  
 $U_{ss}$ : equilibrium potential of the electrode on the surface [V]  
 $U$ : equilibrium potential of the electrode [V]  
 $D_{s,eff}$ : effective solid-phase diffusion coefficient [ $m^2 \cdot s^{-1}$ ]  
 $D_{e,eff}$ : effective electrolyte diffusion coefficient [ $m^2 \cdot s^{-1}$ ]  
 $R_p$ : radius of the solid-phase particle [m]  
 $a_s$ : specific surface area of electrode [ $\varepsilon_s/R_p$ ][ $m^{-1}$ ]  
 $\varepsilon_s$ : volume fraction of the solid phase [-]  
 $\varepsilon_e$ : porosity or volume fraction of the electrolyte [-]  
 $\sigma_{eff}$ : effective solid-phase conductivity [ $S \cdot m^{-1}$ ]  
 $\kappa_{eff}$ : effective electrolyte (ionic) conductivity [ $S \cdot m^{-1}$ ]  
 $k_{eff}$ : effective reaction rate constant [ $A \cdot m^{2.5} \cdot mol^{-1.5}$ ]  
 $L$ : thickness of a domain [m]  
 $r_f$ : SEI film resistance [ $\Omega \cdot m^2$ ]  
 $F$ : Faraday constant [ $s \cdot A \cdot mol^{-1}$ ]  
 $T$ : cell temperature [K]  
 $T_{ref}$ : reference temperature [K]  
 $R_g$ : universal gas constant [ $J \cdot K^{-1} \cdot mol^{-1}$ ]  
 $t_a^0$ : transference number ( $= 1 - t_c^0$ ) [-]  
 $f_{c/a}$ : the mean molar activity coefficient in the electrolyte  
 $[-]$   $\alpha$ : transport coefficients,